

Temperature variations of the disorder-induced vortex-lattice melting landscape

A. Soibel¹, Y. Myasoedov¹, M. L. Rappaport¹, T. Tamegai^{2,3}, S. S. Banerjee¹, and E. Zeldov¹

¹*Department of Condensed Matter Physics, The Weizmann Institute of Science, Rehovot 76100, Israel*

²*Department of Applied Physics, The University of Tokyo, Hongo, Bunkyo-ku, Tokyo 113-8656, Japan*

³*CREST, Japan Science and Technology Corporation (JST), Japan*

(November 1, 2018)

Differential magneto-optical imaging of the vortex-lattice melting process in $\text{Bi}_2\text{Sr}_2\text{CaCu}_2\text{O}_8$ crystals reveals unexpected effects of quenched disorder on the broadening of the first-order phase transition. The melting patterns show that the disorder-induced melting landscape $T_m(H, \mathbf{r})$ is not fixed, but rather changes dramatically with varying field and temperature along the melting line. The changes in both the scale and shape of the landscape are found to result from the competing contributions of different types of quenched disorder which have opposite effects on the local melting transition.

PACS numbers: 74.60.Ec, 74.60.Ge, 74.60.Jg, 74.72.Hs

In recent years, phase transitions in the vortex-matter have been the subject of numerous theoretical and experimental investigations [1]. In particular, significant progress has been achieved in experimental identification of the factors that determine the mean-field location of the first-order melting transition on the $H - T$ phase diagram. It has been shown that weak point disorder shifts the melting transition to lower temperatures while preserving its first-order nature [2,3]. Alternatively, presence of correlated disorder tends to shift the transition to higher temperatures [4,5]. Oxygen doping, furthermore, changes the material anisotropy and significantly alters the slope of the melting line [6,7]. In sharp contrast to the extensive knowledge of the mean-field behavior, no information is currently available on the factors that determine the *local* properties and fluctuations of the phase transition. Since all the parameters that determine the mean-field transition line $T_m(H)$ presumably have considerable variance in their local values, the local melting temperature, or melting landscape, $T_m(H, \mathbf{r})$, should exhibit significant local fluctuations, which generally lead to rounding of a first-order transition [8]. Consequently, instead of undergoing a sharp melting transition in the entire volume of the sample, the vortex-lattice may display a non-trivial phase separation, the detailed mechanism of which is unknown. Broadening mechanisms of the first-order transition are of significant general interest in condensed matter physics [8]. However, their experimental study on an atomic scale is formidable. The vortex system can therefore serve as an invaluable tool for direct investigation of the local thermodynamic behavior at phase transitions in the presence of quenched disorder.

In this Letter we present the first experimental study of the effects of disorder on the local melting process at various points along the first-order transition line. Variations in quenched material disorder and anisotropy change the local vortex potential and elastic moduli, thus creating a complicated melting landscape $T_m(H, \mathbf{r})$ in the sample.

Using the recently developed differential magneto-optical (MO) imaging [9] we have obtained a direct visualization of the melting landscape in $\text{Bi}_2\text{Sr}_2\text{CaCu}_2\text{O}_8$ (BSCCO) crystals. In contrast to what may be expected, the disorder-induced landscape is not constant, but rather varies profoundly with changing temperature along the melting line. It is found that the valleys of the landscape may turn into peaks and that the characteristic length-scale of potential fluctuations increases by an order of magnitude with decreasing temperature. These unexpected changes in both the scale and shape of the melting landscape are shown to arise from competing contributions of various types of disorder which influence the melting transition differently.

The experiments were carried out on various BSCCO crystals [7] ($T_c = 91$ K) with typical dimensions $1 \times 1 \times 0.05$ mm³. In contrast to the conventional MO technique [10], in differential MO imaging the applied field H_a is modulated by a small amount $\delta H_a \ll H_a$ and the corresponding differential signal is acquired using a CCD camera and averaged over many cycles [9]. This method improves the sensitivity by about two orders of magnitude, yielding field resolution of about 30 mG. In this work, we have used an additional method, in which the sample temperature T is modulated by a small $\delta T \simeq 0.25$ K at a typical rate of 10^{-3} Hz. The measurements were carried out by sweeping the temperature or field both up and down through the transition with either type of modulation. In the presented sample no irreversible effects or hysteresis were observed throughout the melting transition (compare with Fig. 4 in Ref [9]).

The vortex-lattice melting is a first-order transition at which the local field B in the liquid phase increases discontinuously by ΔB relative to the solid [11]. On increasing the temperature by δT , additional liquid droplets are nucleated within the solid and the existing liquid domains expand. In the differential image these new liquid regions appear as bright areas in which the field is enhanced by $\Delta B \simeq 0.2$ G. Figure 1 shows four examples of the differ-

ential melting patterns at four different points along the melting line. In all images liquid phase occupies about 50% of the crystal volume. There are two striking observations in these images: one is that the typical size and shape of the melting patterns change dramatically with increasing field, and the other is that in most of the sample area there is little correlation between the patterns at low and high fields. At $H_a = 20$ Oe the liquid regions form arc-like patterns in the vertical direction. At a lower field, 10 Oe, the arcs fracture into microscopic droplets each containing just a few tens of vortices. At higher fields, in contrast, the patterns become much coarser (40 and 75 Oe images) and gradually lose correlation with the low-field patterns. From 75 Oe to 300 Oe, which is the upper limit of our measurements, the melting patterns show only little change with field (not shown). The melting patterns differ significantly from sample to sample, but in all the investigated crystals similar characteristic changes of the patterns with temperature are found.

Figures 2a and 2b present the evolution of the lattice melting as the temperature is raised at a fixed H_a , the different colors indicating areas which melt upon 0.25 K increments of T . Material disorder modifies the local melting temperature, thus forming a complicated $T_m(H, \mathbf{r})$ landscape. Figures 2a and 2b can thus be viewed as ‘topographical maps’ of the melting landscape at H_a of 20 and 75 Oe, respectively. The minima points and the valleys of the landscape melt first (blue), whereas the peaks of the landscape melt last (red). The two landscapes in Fig. 2 are substantially different. In addition to the significant change in the characteristic lengthscale and roughness of the landscape, there are many regions in the sample that show qualitatively different properties. For example, at 20 Oe the valley in the form of an arc along the ‘O-O’ dashed line has three long and narrow blue segments, while at 75 Oe, the blue minima have a form of rather circular spots. Also, at 75 Oe in the lower-right corner of the sample, to the right of the ‘O-O’ valley, a number of blue and cyan minima are visible. At 20 Oe, on the other hand, this region is rather ‘elevated’, characterized by green and yellow colors. In the top part of the sample a yellow ‘ridge’ is clearly visible along the ‘P-P’ line in Fig. 2b, whereas in Fig. 2a this ridge is absent. At 75 Oe, on the right-hand-side of the ridge, there is an extended peak (orange), whereas in the corresponding region at 20 Oe, blue and green valleys are seen. Also, importantly, the width of the transition or the valley-to-peak height, changes significantly. At 20 Oe the entire sample melts within about 1 K, whereas at 75 Oe the melting process spans almost twice this range.

For a more quantitative analysis we have inspected the melting behavior at several points, e.g., points A and B in Fig. 2. The melting lines $T_m(H)$ at these two points are shown in Fig. 3a. There is a systematic divergence of the two melting lines that is seen most clearly in Fig. 3b in the form of their difference $T_{mB} - T_{mA}$ versus the

mean-field T_m . Close to T_c , point B melts 0.5 K below point A whereas at lower temperatures the behavior is inverted and point B melts about 2 K above point A. The two melting lines intersect at about 85 K. There are numerous other points in the sample that show intersecting melting lines, which means that regions which are valleys of the landscape at low fields may turn into peaks at high fields and vice versa. Figure 3c shows the width of the melting transition of the entire sample, which is the first direct measurement of the degree of global rounding of the first-order transition along the melting line. At high temperatures the vortex lattice melts within about 1 K whereas at low temperatures the transition width reaches about 5 K. All these findings show that the melting properties change significantly along the melting line.

There are two main factors that determine the observed melting behavior: one is the disorder-induced melting landscape and the other is the solid-liquid surface tension σ . We analyze first the effect of surface tension. The minimum nucleation radius r of a liquid droplet is determined by the balance between the free energy gain at the transition $\Delta F = (\partial F_s/\partial H - \partial F_l/\partial H)h\pi r^2 d = \Delta B h r^2 d/4$ and the energy cost of the interface creation $2\pi\sigma r d$, which results in $r = 8\pi\sigma/\Delta B h$ [9]. Here $h = H - H_m(T)$ is the degree of superheating, d is the sample thickness, and the difference in the derivatives of the free energies in the solid and liquid phases is given by $\partial F_s/\partial H - \partial F_l/\partial H = \Delta B/4\pi$. The surface tension can be estimated [9] as $\sigma \simeq \eta a_0 H_m \Delta B/4\pi$, where η is a numerical prefactor, $a_0 \simeq (\phi_0/H)^{1/2}$ is the intervortex spacing, and ϕ_0 is the flux quantum. σ is thus expected to grow as $H_m^{1/2}$ and hence the size of the nucleating liquid droplets should increase accordingly as $r \simeq 2\eta(\phi_0 H_m)^{1/2}/h$. Thus the increase with field of the characteristic size of the liquid patterns in Figs. 1 and 2 could possibly be attributed to the increase in the surface tension. However, the above estimate of the contribution of the surface tension was carried out without disorder. In the presence of disorder the variations in the nucleation radius due to a change in σ are expected to be reduced. In contrast, inspection of the 10 and 75 Oe patterns in Fig. 1, for example, indicates that the increase in the characteristic droplet size is substantially larger than the anticipated $(7.5)^{1/2} = 2.74$. Furthermore, the fact that above 75 Oe, up to 300 Oe, the scale does not change with field is inconsistent with the surface tension scenario. Yet the most compelling argument against the dominant role of σ is the following. Surface tension should act as a short-range filter that smears out the fine structure of the melting landscape, but preserves the long-range correlations. Analysis of the melting patterns shows that this is not the case, and both the short and long range correlations are lost with increasing H_a . In addition, it is highly unlikely that surface tension can cause the local melting lines to cross as in Fig. 3 and to change macroscopic valleys into peaks and vice versa. Finally, a larger σ should sharpen the overall

melting transition by cutting off the tails of the disorder-induced distribution function of the melting landscape [8], in contrast to the observed broadening of the transition with increasing H_a (Fig. 3c). We therefore conclude that the observed changes in the melting patterns are mainly caused by changes in the disorder-induced potential landscape. This conclusion is consistent with the previous assessment of a very low solid-liquid surface tension [9].

We now address the possible mechanisms for the variations in the potential landscape. For this it is convenient to parameterize the local melting curves using the generic expression of the melting transition [12], $H_m(T, \mathbf{r}) = H_0(\mathbf{r})(1 - T/T_c(\mathbf{r}))^\alpha$. We find that $\alpha(\mathbf{r})$ depends weakly on location, and hence set $\alpha(\mathbf{r}) = \alpha$ for simplicity. Defining $T_c(\mathbf{r}) = T_c + \Delta T_c(\mathbf{r})$ and $H_0(\mathbf{r}) = H_0 + \Delta H_0(\mathbf{r})$, we rewrite $H_m(T, \mathbf{r}) = H_m(T) + \Delta H_m(T, \mathbf{r})$, where $H_m(T) = H_0(1 - T/T_c)^\alpha$ is the mean-field melting line, and $\Delta H_m(T, \mathbf{r}) \simeq [\Delta H_0(\mathbf{r}) + \alpha H_0 \Delta T_c(\mathbf{r}) / (T_c - T)](1 - T/T_c)^\alpha$ describes the disorder-induced melting landscape. $\Delta H_m(T, \mathbf{r})$ has two terms: the first results from variations in the slope of the melting line $\Delta H_0(\mathbf{r})$ and the second from variations in the local T_c . Due to the diverging $T_c - T$ denominator the second term should become dominant near T_c , whereas the first term may dominate at low temperatures. Analysis of the local melting lines at various locations across the sample results in the following parameters: $H_0 = 900$ Oe, $\Delta H_0 = 80$ Oe, $T_c = 95$ K, $\Delta T_c = 0.7$ K, and $\alpha = 1.6$. Using these values we find that the two terms of $\Delta H_m(T, \mathbf{r})$ become comparable at $T \simeq 82$ K. This result explains a number of observed features: Since at low temperatures $\Delta H_0(\mathbf{r})$ is the dominant term, the form of the landscape becomes temperature and field independent, explaining the invariance of the melting patterns above 75 Oe. However, the amplitude of the landscape fluctuations increases as $(1 - T/T_c)^\alpha$ with decreasing temperature, thus explaining the continuous broadening of the transition width in Fig. 3c. When the two terms of $\Delta H_m(T, \mathbf{r})$ become comparable above ~ 82 K there is a gradual crossover to a new landscape. As a result, the melting patterns change significantly and lose their spatial correlations as seen in Fig. 1. At higher temperatures the ΔT_c variations should eventually become the dominant parameter which governs the shape and the scale of the melting patterns. One can check the self-consistency of this argument as follows. At high temperatures ΔT_c should also modify the local critical field $H_{c1}(\mathbf{r})$ and the corresponding value of the local penetration field. Figure 2c shows a high-sensitivity image of the initial field penetration into the sample at $H_a = 2$ Oe and $T = 89$ K. A strong correlation between the penetration form and the melting patterns at low fields is readily visible. For a more accurate comparison Fig. 2d presents a superposition of the penetration image with the melting patterns at 20 Oe. The color in the image is given by the melting

contours, while the brightness is defined by the penetration field. It is clearly seen that most of the macroscopic blue regions of liquid nucleation coincide with the bright areas where the field penetrates first. In particular, the correspondence between the arc structures of the penetration field and the melting contours is remarkable. This correspondence indicates that the melting propagation at low fields is indeed governed by the local variations in T_c . It is interesting to note that a comparison between the penetration image and the melting contours at $H_a = 75$ Oe results in a surprisingly large anti-correlation behavior: The regions into which the field penetrates first are often the last ones to melt. Such anti-correlation is clearly seen, for example, for the ‘P-P’ strip which is bright in Fig. 2c but is mainly yellow and orange in Fig. 2b. The anti-correlation behavior causes the observed crossing of the local melting lines as in Fig. 3 and results in the variable melting landscape.

It is interesting to understand which types of material disorder contribute to the different trends of the melting landscape. Variations in pinning by point disorder may locally destabilize the lattice, resulting in landscape minima. Local correlated disorder, in contrast, is expected to stabilize the lattice, creating maxima points of the landscape. However, such pinning disorder is not expected to produce appreciable ΔT_c variations, nor should it result in crossing of the local melting lines. Variations in the oxygen stoichiometry or in cation ratio, on the other hand, could give rise to both effects. Oxygen doping modifies both the T_c and the anisotropy. In overdoped domains T_c is suppressed, but the corresponding reduction in anisotropy results in a larger slope of $H_m(T)$ which may in turn lead to the crossing of the local melting lines. Our analysis of the crystal growth conditions indicates that the arc structures in Fig. 2 are related to a slight modulation in material composition and to the curved form of the meniscus between the solid and liquid phases of BSCCO during the floating zone crystallization process. We have also carried out preliminary X-ray spectroscopy microanalysis [13] which indicates some correlation between small variations in the Sr/Cu ratio and the melting patterns. This finding further indicates that the complexity of the melting is related to the sample disorder and inhomogeneities. However, the specific influence of the disorder still needs further investigation since the same variation in Sr concentration, for example, can have different microscopic effects depending on the exact site occupied by excess Sr.

We thank D.E. Feldman and V.B. Geshkenbein for valuable discussions. This work was supported by the Israel Science Foundation and Center of Excellence Program, by Minerva Foundation, Germany, by the Ministry of Science, Israel, and by the Grant-in-Aid for Scientific Research from the Ministry of Education, Science, Sports and Culture, Japan. EZ acknowledges the support by the Fundacion Antorchas - WIS program.

-
- [1] G. Blatter *et al.*, Rev. Mod. Phys. **66**, 1125 (1994).
 - [2] B. Khaykovich *et al.*, Phys. Rev. B **56**, R517 (1997).
 - [3] L. M. Paulius *et al.*, Phys. Rev. B **61**, R11910 (2000).
 - [4] B. Khaykovich *et al.*, Phys. Rev. B **57**, R14088 (1998).
 - [5] W. K. Kwok *et al.*, Phys. Rev. Lett. **84**, 3706 (2000).
 - [6] B. Khaykovich *et al.*, Phys. Rev. Lett. **76**, 2555 (1996).
 - [7] S. Ooi *et al.*, Physica C **302**, 339 (1998).
 - [8] Y. Imry and M. Wortis, Phys. Rev. B **19**, 3580 (1980).
 - [9] A. Soibel *et al.*, Nature **406**, 282 (2000).
 - [10] For a recent review see: A. A. Polyanskii *et al.*, NATO Science Series **3/72**, 353 (Kluwer Academic Publishers, Dordrecht, 1999).
 - [11] E. Zeldov *et al.*, Nature **375**, 373 (1995).
 - [12] G. Blatter and B. I. Ivlev, Phys. Rev. B **50**, 10272 (1994).
 - [13] T. Tamegai, M. Yasugaki, K. Itaka, and M. Tokunaga, Physica C **357-360**, 568 (2001).

FIGURE CAPTIONS

Fig. 1. Differential MO images of the vortex-lattice melting in BSCCO crystal at four points along the melting line: $H_m(T) = 10$ Oe (89.5 K), 20 Oe (86.75 K), 40 Oe (82.0 K), and 75 Oe (75.25 K). The differential images are obtained by subtracting the image at $T - \delta T/2$ from the image at $T + \delta T/2$, with $\delta T = 0.25K$.

Fig. 2. The contours of the melting propagation at $H_a = 20$ Oe (a) and 75 Oe (b). The color code indicates the expansion of the liquid domains as the temperature is increased in 0.25 K steps. The onset of melting is at $T_m^{on} = 86.25$ K in (a) and at 74.25 K in (b). (c) Differential magneto-optical image of the magnetic field penetration at $H_a = 2$ Oe, $T = 89$ K, $\delta H_a = 1$ Oe. (d) Superposition of (a) and (c).

Fig. 3. (a) Local melting lines at points A (\times) and B (\circ) indicated in Fig. 2. (b) Difference of the melting temperatures at points B and A vs. the average melting temperature. (c) The full width of the melting transition vs. temperature.

This figure "Fig1_nw2.jpg" is available in "jpg" format from:

<http://arxiv.org/ps/cond-mat/0108299v1>

This figure "Fig2_nw2.jpg" is available in "jpg" format from:

<http://arxiv.org/ps/cond-mat/0108299v1>

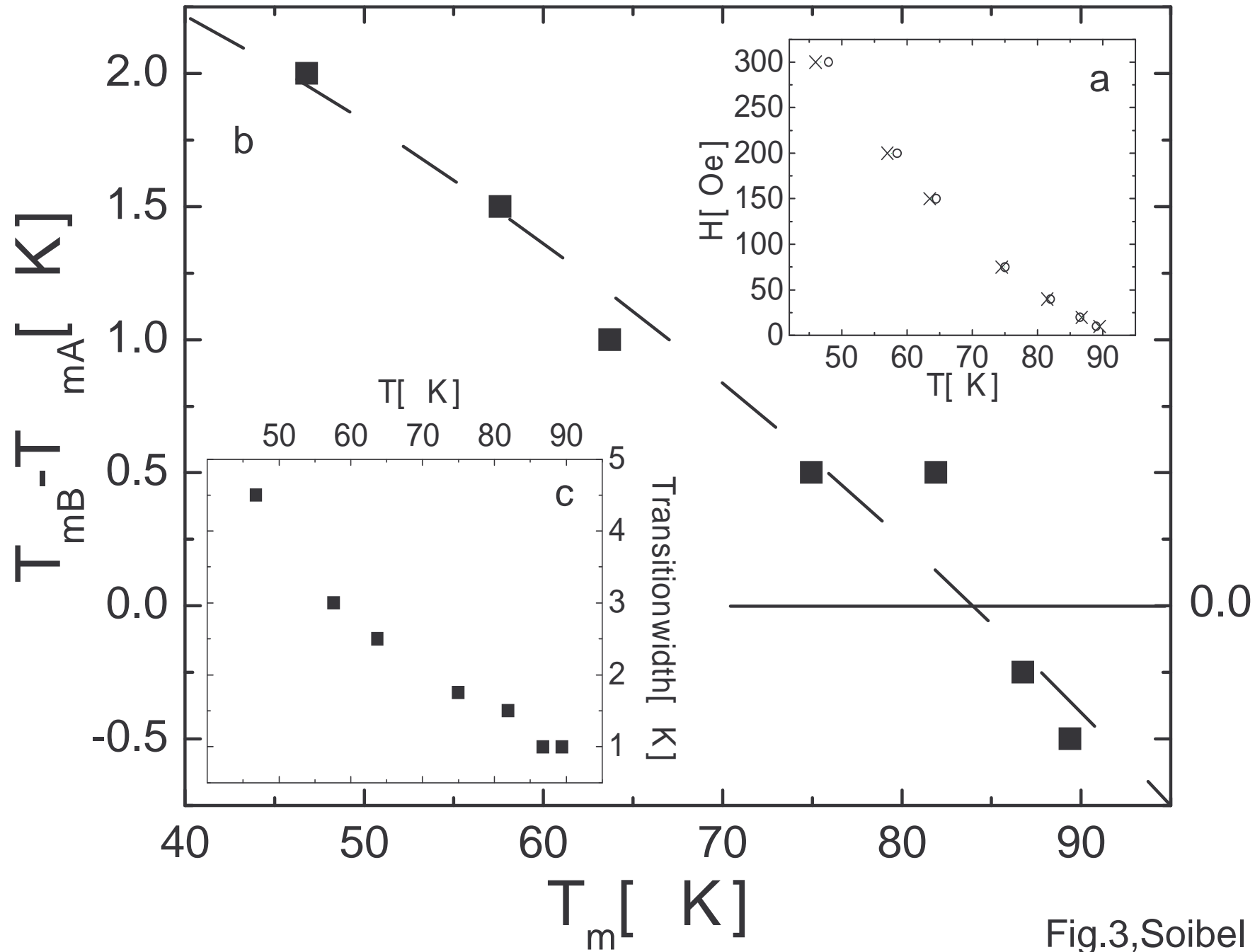


Fig.3, Soibel *etal.*